MAGNETISM
AND FERROELECTRICITY

Parameters of the Potential Well of an Off-Center Ge Atom in a GeTe–SnTe Solid Solution

A. I. Lebedev and I. A. Sluchinskaya

Moscow State University, Vorob'evy gory, Moscow, 119992 Russia
e-mail: swan@scon155.phys.msu.su
Received September 11, 2006

Abstract—An method is proposed for determining the shape of the three-dimensional multiwell potential of an off-center atom from EXAFS data. The parameters of the potential well of a Ge atom in GeTe and $Sn_{1-x}Ge_xTe$ ($x \geq 0.4$) are determined in the classical and quantum-mechanical approximations. The potential-well depth is varied in the interval 20–40 meV depending on the Ge content, which indicates that the phase transition in these crystals is intermediate in character between the displacement and order–disorder transitions. From analyzing the conditions for the applicability of the classical approximation, it follows that quantum effects must be taken into account in determining the parameters of the potential well of an off-center Ge atom in $Sn_{1-x}Ge_xTe$. Quantum-mechanical calculations show that the energy of the lower level in the vibration spectrum of the Ge atom coincides with the maximum energy in the potential well to within several millielectron-volts. The high probability of tunneling or an over-barrier transition of the off-center atom between the potential-well minima prevents dipole reorientations from being frozen at low temperatures.

PACS numbers: 61.10.Ht, 61.72.-y, 77.84.Bw

DOI: 10.1134/S1063783407060194

1. INTRODUCTION

Considerable interest in studying off-center impurity atoms is related to the fact that the presence of these atoms in crystals can induce ferroelectric phase transitions (PTs) [1]. To explain the properties of such PTs at the microscopic level, it is necessary to know the shape of the potential wells of off-center impurity atoms.

In a microscopic one-dimensional ferroelectricity model, the Hamiltonian has the well-known form [2]

$$\hat{H} = \sum_i \left(\frac{1}{2M} p_i^2 + \frac{A}{2} x_i^2 + \frac{B}{4} x_i^4 \right) + \frac{C}{2} \sum_{i,j} (x_i - x_j)^2 - E \sum_i x_i, \tag{1}$$

where M is the atomic mass; x_i and p_i are the coordinate and momentum of an atom, respectively; E is the strength of an external electric field; and A, B, and C are parameters. Equation (1) can be written as a sum of independent equations describing the motion of one atom in an effective potential:

$$\hat{H} = \sum_i \left[\frac{1}{2M} p_i^2 + \left(\frac{A+2C}{2} x_i^2 + \frac{B}{4} x_i^4 \right) - x_i \left(C \sum_{j \neq i} x_j + E \right) \right]. \tag{2}$$

Potential (2) consists of the following two terms: the local anharmonic potential $((A + 2C)/2)x^2 + (B/4)x^4$ and the term describing the interaction of the atom under consideration with the other atoms and the external field. If quantum effects are neglected, the necessary condition for a PT to occur in the crystal is $A < 0$ in the microscopic model [2]. In this case, the local potential has two equivalent minima (in the three-dimensional case, up to eight minima, depending on the symmetry of the site occupied by the atom). Using Eq. (1), the displacement and order–disorder PTs can be described in the framework of a unified approach.

Within the microscopic model, the character of a PT (order–disorder or displacement transition) in a simple cubic lattice is determined by the ratio between the following two characteristic energies [2]: the well depth $U_w = A^2/4B$ and the "binding energy" $U_b = 6|A|C/B$, which is equal to the energy required for the atom to move from the bottom of the well to the potential-well maximum (at $x = 0$) under the condition that all the other atoms remain in the ordered state. The dimensionless parameter $s = U_w/U_b$ determines the properties and dynamics of the PT; namely, the PT is of the order–disorder type for $s \gg 1$ and of the displacement type for $s \ll 1$. In the microscopic model, the PT temperature is $kT_c \approx (3/\ln 2)|A|C/B$ in the limit $s \gg 1$ and $kT_c \approx (8\pi/3)|A|C/B$ in the limit $s \ll 1$ [3]. Therefore, one can assume that $U_b \approx kT_c$ and, consequently, $s \approx U_w/kT_c$. Thus, we need to know the potential-well depth in order to determine the type of the PT.

In real ferroelectrics, PTs can rarely be assigned to the displacement or order–disorder type; more frequently, PTs in them are of the intermediate type. The problem of determining the type of a PT can be solved using its properties, such as the Curie constant, the existence of a soft mode, and the behavior of the heat capacity near T_c. However, it is often difficult to interpret the measurement results, because the soft mode decays, the behavior of the heat capacity is distorted in the presence of defects, and it is difficult to conduct dielectric measurements in samples with high conductivity. A direct determination of the parameters of microscopic Hamiltonian (1) would be a solution of this problem. This is of fundamental importance for understanding of the nature of PTs in crystals and for the prediction of the PT properties.

The GeTe–SnTe system is an example of a system for which studies yield contradictory information on the PT type. The components of this system form a continuous series of solid solutions with a NaCl-type structure in the high-temperature phase. In a $Sn_{1-x}Ge_xTe$ solid solution, the temperature of the PT to the rhombohedral ferroelectric phase increases from ~100 to 700 K with increasing x [4]. Precision x-ray studies of lattice distortions below T_c [5] have shown that the order of the PT in these crystals changes with increasing x; namely, the transition is of the second order for $x < 0.28$ and of the first order for $x > 0.28$. The behavior of the heat capacity [6] and elastic moduli [7] near the Curie point demonstrate that the PTs are of the displacive type (in GeTe, in addition, a soft mode was observed [8]). However, extended x-ray-absorption fine-structure (EXAFS) studies [9] have shown that Ge atoms are displaced from lattice sites both below and above T_c, which indicates that these atoms are in a multiwell potential and that the PT is of the order–disorder type. These contradictory data and the simplicity of the crystal structure (with two atoms in the primitive cell) prompted us to use EXAFS spectroscopy to study the shape of the potential well of Ge atoms in $Sn_{1-x}Ge_xTe$. The proposed method can also be useful for studying more complicated ferroelectrics.

2. DESCRIPTION OF THE METHOD

EXAFS spectroscopy is a powerful method for studying the local structure of crystals. It has been used to answer the question of whether the potential in some ferroelectrics are of the single-well or multiwell type [10–15]. The solution of this problem is reduced to studying the atomic motion in a strongly anharmonic crystal.

To date, the parameters of single-well potential anharmonicity have been determined from the EXAFS data using the cumulant expansion method [16]. However, this method can be applied if the anharmonicity is not very strong and, hence, one can restrict oneself to only several first terms of an expansion in powers of k.

In addition, this method is inapplicable to crystals whose potential has several minima and it does not yield information on the atomic-motion anisotropy. Because the potential of an off-center impurity atom has several energetically equivalent minima, another approach is required to solve our problem.

In this paper, we propose a new method for solving the problem of determining the multiwell-potential parameters for off-center impurities. This method is free from the drawbacks inherent in the cumulant expansion method. The basic special features of this approach are the following: (i) In calculating the theoretical EXAFS function, exact three-dimensional integration is performed, which makes it possible to consider potentials with an arbitrary degree of anharmonicity. (ii) A cluster is chosen with an atomic arrangement coinciding with that in the first coordination shell of an absorbing atom, which allows one to consider multiwell potentials and determine the parameters of the atomic-motion anisotropy.

In the single-scattering approximation of EXAFS theory, the oscillating part of the spectrum at the K-absorption edge (the EXAFS function) can be written as follows [17]:

$$\chi(k) = \sum_j \frac{S_0^2}{k} \text{Im}\left\{ f(k, \pi) e^{2i\delta_1} \int \frac{\rho(\mathbf{r}_j) e^{-2r_j/\lambda}}{r_j^2} e^{2ikr_j} d\mathbf{r}_j \right\}, (3)$$

where summation is over all nearest neighbors; S_0^2 is the factor taking into account many-electron effects and inelastic scattering; f is the backscattering complex function; δ_1 is the phase of the photoelectron escaping from the absorbing atom; λ is the photoelectron mean free path; k is the photoelectron wave vector, which is related to the absorbed photon energy E and the photoionization energy E_0 by the formula $k = \sqrt{2m(E - E_0)}/\hbar$; $\rho(\mathbf{r})$ is the probability that the scattering atom is at the point $\mathbf{r}$ (the position of the absorbing atom is taken to be the origin of the reference system); and $r = |\mathbf{r}|$ is the distance between the absorbing and scattering atoms. The quantities S_0^2, f, δ_1, and λ characterize the absorbing and scattering atoms. The distribution function $\rho(\mathbf{r})$ contains information on the local structure and motion of atoms.

Since the function $\rho(\mathbf{r})$ is determined by $V(\mathbf{r})$, the potential-well parameters can be found from the EXAFS spectra. In our approach, the EXAFS spectra are processed as follows. We first parametrize the three-dimensional potential $V(\mathbf{r})$, taking the crystal symmetry into account. Then, we calculate the normalized distribution function $\rho(\mathbf{r})$ and substitute it into Eq. (3) in order to calculate the theoretical EXAFS spectrum and compare it with an experimental one. Varying the potential parameters and repeating the procedure for calculating the theoretical spectrum, we next minimize the root-mean-square (rms) deviation of the theoretical
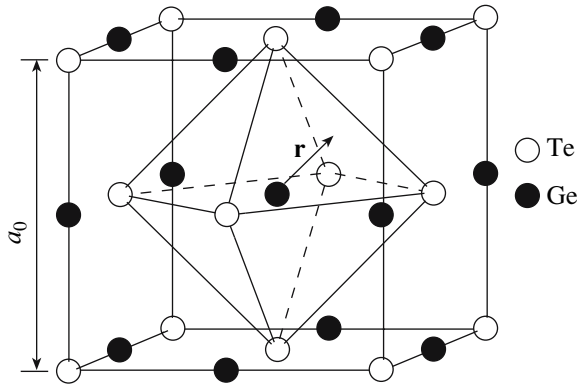
Fig. 1. Fragment of the fcc lattice with a Ge atom moving in the octahedron formed by Te atoms.

EXAFS spectrum from the experimental one and thus determine the shape of the potential well.

Above the PT temperature, our crystals have a NaCl-type structure shown in Fig. 1. In this structure, each off-center Ge atom moves in the octahedron formed by six Te atoms. In ferroelectrics, the displacement of ferroelectrically active atoms from lattice sites due to thermal motion is always greater than that of surrounding atoms. Therefore, the thermal motion of Te atoms can be neglected and only the motion of the Ge atom in the rigid octahedron can be considered in a first approximation. In our experiments, the Ge atoms absorb x-ray radiation and the scattering atoms are Te atoms. Since we are interested in the motion of Ge atoms, it is appropriate to single out a cluster consisting of seven atoms (Ge + 6Te) and pass to a new reference system whose origin is located at the octahedron symmetry center. Taking into account that $\rho(\mathbf{r})$ is the pair distribution function, we can rewrite Eq. (3) in the new reference system and show that the expression for $\chi(k)$ remains the same except for the fact that the vector $\mathbf{r}$ is now the coordinate of the Ge atom and $\rho(\mathbf{r})$ is the probability that the Ge atom is at the point $\mathbf{r}$. In the new reference system, Te atoms are located at the distance $a_0/2$ from the origin of coordinates along the $\langle 100 \rangle$ axes (a_0 is the lattice parameter). Therefore, for the Ge atom located at the point $\mathbf{r} = (x, y, z)$, the contribution of the six Te atoms to EXAFS function (3) can be expressed in terms of six three-dimensional integrals in which the distances r_j are calculated from the formulas $r_{1,2}^2 = (a_0/2 \pm x)^2 + y^2 + z^2$, $r_{3,4}^2 = x^2 + (a_0/2 \pm y)^2 + z^2$, and $r_{5,6}^2 = x^2 + y^2 + (a_0/2 \pm z)^2$.

As was mentioned above, the potential $V(\mathbf{r})$ consists of two parts, namely, the local anharmonic potential $V_{loc}(\mathbf{r})$ and the term $V_{mf} = (\mathbf{d} \cdot \mathbf{E}_{mf})$, which describes the interaction of the atom with the other atoms and the external field. We expand the potential $V_{loc}(\mathbf{r})$ in powers of the atomic displacement components in the neigh-

borhood of the origin of coordinates. For a site characterized by the point symmetry group O_h, the expansion in a power series up to fourth-order terms has the form

$$V_{loc}(\mathbf{r}) = \alpha + \beta r^2 + \gamma r^4 + \delta(x^2 y^2 + x^2 z^2 + y^2 z^2),$$
$$r^2 = x^2 + y^2 + z^2, \tag{4}$$

where α, β, γ, and δ are coefficients. Because the distribution function is independent of the choice of the zero of energy, we set $\alpha = 0$. Then, Eq. (4) can be rewritten as

$$V_{loc}(\mathbf{r}) = a(-2R_{min}^2 r^2 + r^4)$$
$$+ d\left(x^2 y^2 + x^2 z^2 + y^2 z^2 - \frac{r^4}{3} \right), \tag{5}$$

where $a = \gamma + \delta/3 > 0$ is the parameter characterizing the isotropic part of the fourth-order anharmonicity, $R_{min}^2 = -\beta/(2\gamma + 2\delta/3)$ is the square of the distance to the potential minimum, and $d = \delta$ is the parameter describing the anisotropic part of the fourth-order anharmonicity. As mentioned above, the Ge atoms are displaced in a $\langle 111 \rangle$ direction (one of the eight equivalent minima) in the low-symmetry phase of $Sn_{1-x}Ge_xTe$; therefore, we have $d < 0$. The quantities a, R_{min}^2, and d are the parameters of the local anharmonic potential in Eq. (2), which is generalized to the three-dimensional case.

The experimental data discussed in this paper are obtained for samples in the ferroelectric phase. Therefore, it is necessary to take into account the existence of a preferential direction (the term V_{mf} and a rhombohedral distortion of the lattice in the processing of the data. We now estimate the effect of these factors and the higher order invariants on the obtained results. The inclusion of the rhombohedral lattice distortion (known from experiment) in the data processing did not have a significant effect on the agreement between the experimental and theoretical spectra and on the values of the local-potential parameters. The inclusion of the sixth-order invariants in expansion (4) shows that their influence on the results obtained at least for a low temperature is also insignificant. As for the molecular field $\mathbf{E}_{mf}$, its influence on the potential parameters can be noticeable. However, the inclusion of this field in the set of fitting parameters in the data processing had almost no effect (the agreement between the experimental and theoretical spectra depended on $\mathbf{E}_{mf}$ only slightly). For this reason, we neglect the rhombohedral distortion, the sixth-order invariants, and the influence of the molecular field in this study.

If the measurement temperature exceeds the Debye temperature and the classical approximation can therefore be used, then the probability of finding the atom at an arbitrary point of the crystal is determined by the potential energy at this point, $\rho(\mathbf{r}) \sim \exp[-V(\mathbf{r}/kT)]$. At lower temperatures, it is necessary to take into account

the quantum character of the atomic motion. In this case, the relation between $\rho(\mathbf{r})$ and $V(\mathbf{r})$ becomes more complicated (see Section 5). The classical-approximation calculations are discussed in Section 4. In Section 5, we calculate the vibration spectrum of a Ge atom moving in the obtained anisotropic multiwell potential. By comparing the distribution functions calculated in the classical approximation and using the rigorous quantum-mechanical approach, we show that these functions are essentially different and, consequently, the determination of the potential parameters requires a quantum-mechanical approach. The data obtained within the quantum-mechanical approach are given in Section 6.

3. EXPERIMENT

Measurements were made on polycrystalline $Sn_{1-x}Ge_x Te$ solid solution samples with $x = 0.4$, 0.7, and 1.0. The samples were obtained by alloying binary compounds and subsequent homogenizing annealing at 620°C for 48 h. Immediately prior to measurements, the samples were ground into a powder, which was sieved afterwards. The powdered material was deposited on an adhesive tape. The absorbing-layer thickness optimum for recording spectra was obtained by folding this tape 8 to 16 times.

The EXAFS spectra at the Ge K-absorption edge (11.103 keV) were recorded at station 7.1 of the synchrotron radiation source (SRS, Great Britain) with an electron energy of 2 GeV and a current of 240 mA. Radiation was monochromatized using a Si (111) double-crystal monochromator. The spectra were recorded in the transmission geometry. The intensities of the radiation incident on (I_0) and transmitted through (I_t) the sample were measured by ionization chambers. The samples were placed into a nitrogen cryostat whose temperature could be varied in the temperature range from 77 to 300 K.

The EXAFS function was extracted from the absorption spectra $x\mu(E) = \ln(I_0/I_t)$ (where E is the photon energy) using the traditional method [17, 18]. After subtracting the background due to absorption by other atoms, we extracted the monotonic part of the atom absorption $x\mu_0(E)$ using splines and calculated the dependence of the quantity $\chi(k) = (x\mu - x\mu_0)/x\mu_0$ on the photoelectron wave vector $k = [2m(E - E_0)/\hbar^2]^{1/2}$. The energy corresponding to the inflection point at the absorption edge was taken as the zero of energy E_0. The value of the jump in $x\mu$ at the absorption edge varied from 0.19 to 0.50.

Using the direct and inverse Fourier transforms with a modified Hanning window [17], we extracted the information on the first coordination shell from the experimental $\chi(k)$ curves. The typical range of extraction in the R space was $\Delta R = 1.65$–3.55 Å and that in the k space was $\Delta k = 2.8$–12.7 Å^{-1}. The subsequent data processing included varying the parameters of the prob-
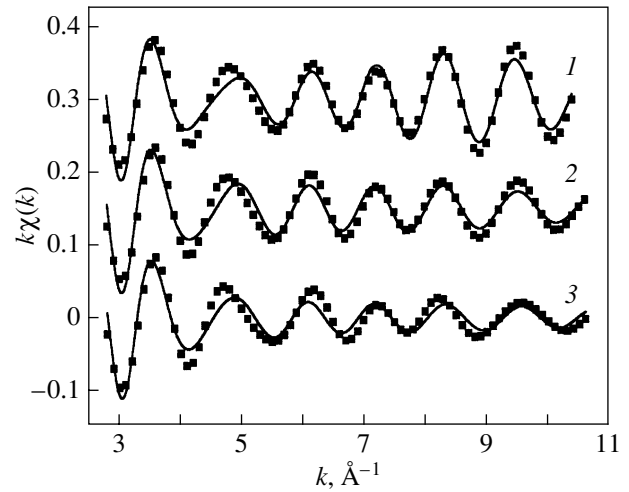

Fig. 2. Comparison of the experimental (points) and theoretical (solid lines) EXAFS spectra for a $Sn_{0.3}Ge_{0.7}Te$ sample at various temperatures T: (*1*) 80, (*2*) 180, and (*3*) 275 K.

lem (a, d, R_{min}^2, S_0^2, a_0, and the shift dE_0 in the zero of energy [17]) to determine their values corresponding to the minimum rms deviation of the theoretical $k\chi(k)$ spectrum from the spectrum extracted from the experimental curve in the way mentioned above. The FEFF computer program [19] was used to find the functions $f(k, \pi)$, $\delta_1(k)$, and $\lambda(k)$ necessary for calculating the theoretical spectra.

As is well known [17], the number of fitting parameters used to analyze the EXAFS data must not exceed the number of independent parameters $N_{ind} = (2/\pi)\Delta R \Delta k$ in the data. In our case, the number of adjustable parameters was six and $N_{ind} = 9$–12.

4. CLASSICAL APPROXIMATION

For a $Sn_{0.3}Ge_{0.7}Te$ sample, the typical EXAFS spectra extracted by the method described above and the best fit to them obtained by the method described in Section 2 are shown in Fig. 2 for three different temperatures. The small discrepancy between the curves is due to the fact that the procedure used to extract the signal from the first coordination shell cannot completely suppress the contribution from the second coordination shell.

Figure 3 shows a cross section of constant-energy surfaces calculated using the obtained parameters of the potential for the sample with $x = 0.7$ at $T = 80$ K. It is seen that the equal-potential curves are substantially elongated in the $\langle 111 \rangle$ direction and the potential energy increases most rapidly for displacements in the $\langle 100 \rangle$ direction.

The temperature dependences of the parameters a, R_{min}^2, and $|d|$ for all $Sn_{1-x}Ge_x Te$ samples under study are given in Figs. 4–6.[1] It is seen from comparing

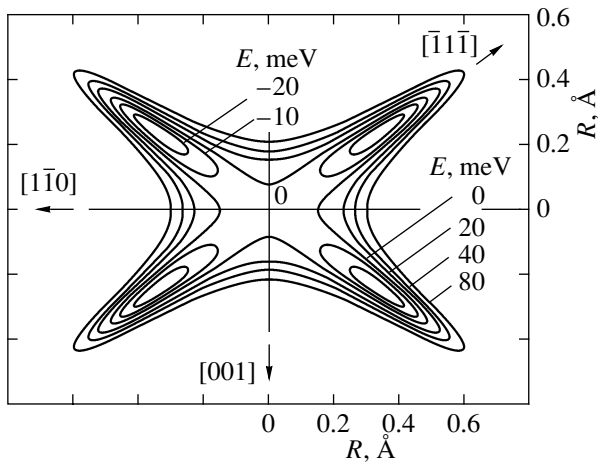**Fig. 3.** Constant-energy surfaces of the potential well in a plane perpendicular to a ⟨110⟩ axis for a $Sn_{0.3}Ge_{0.7}Te$ sample at 80 K.
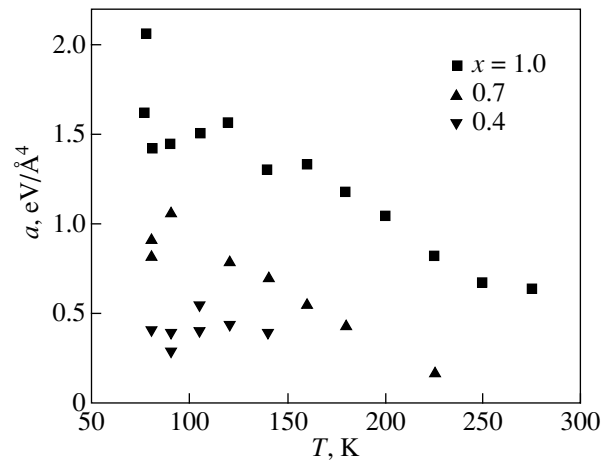
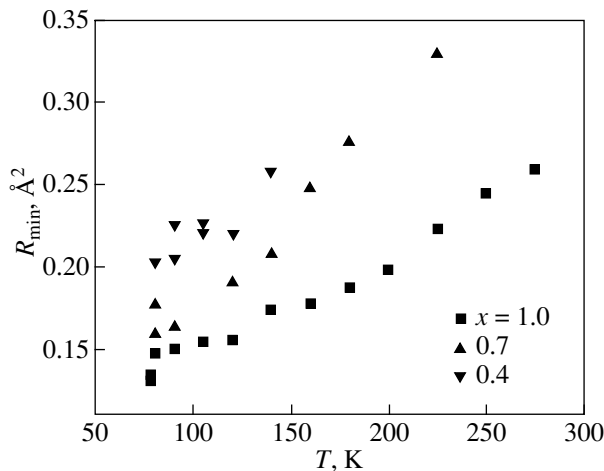**Fig. 4.** Temperature dependence of the parameter a for $Sn_{1-x}Ge_xTe$ samples with various values of x.

Fig. 5. Temperature dependence of the parameter R^2_{min} for $Sn_{1-x}Ge_xTe$ samples with various values of x.

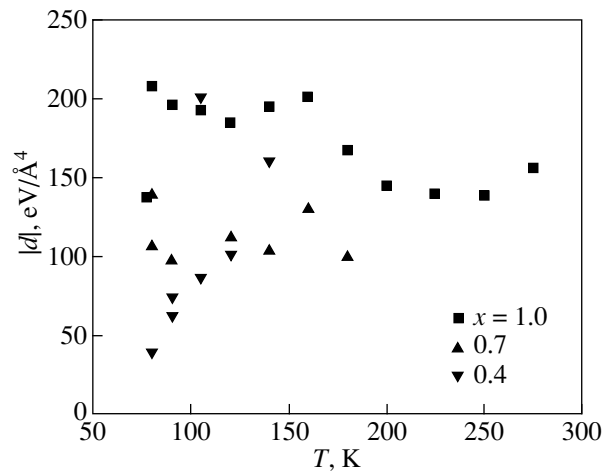**Fig. 6.** Temperature dependence of the parameter d for $Sn_{1-x}Ge_xTe$ samples with various values of x.

Figs. 4 and 6 that the parameter $|d|$ is two orders of magnitude greater than the parameter a. This means that the potential is characterized by strong anisotropy. Indeed, as follows from Eq. (5), the minimum value of the coefficient of r^4 (equal to a) is reached for displacements of the Ge atom in the ⟨111⟩ direction, and the maximum value (equal to $a + |d|/3$), for displacements in the ⟨100⟩ direction. This is not surprising, because the Te atoms near a Ge site are located along the ⟨100⟩ direction and displacements in this direction are accompanied by a strong nonlinear repulsion. At the same time, along the ⟨111⟩ direction, there is a dimple

in the closely packed atomic plane and it is much easier for the off-center Ge atoms to be displaced in this direction (Fig. 1).

As follows from Eq. (5), the potential-well depth is $U_w = aR^4_{min}$. Estimations of U_w give ≈40 meV for the sample with $x = 1$, ≈30 meV for the sample with $x = 0.7$, and ≈20 meV for the sample with $x = 0.4$. Thus, the dimensionless parameter $s = U_w/kT_c$ is about 0.65 for all samples studied. This means that the PT in a $Sn_{1-x}Ge_xTe$ solid solution is intermediate between the displacement and order–disorder types.

We note that, in earlier experimental studies, the off-center atomic displacement discovered above the Curie temperature was associated with an order–disorder PT. However, this conclusion is not unambiguous, because

---

[1] It should be noted that we failed to reliably determine the parameters for a number of spectra recorded at high temperatures. Probably, it is necessary to take sixth-order invariants into account in processing these spectra.

in the microscopic model the type of a PT is determined by the parameter s, as mentioned in Section 1. Thus, in order to prove that a PT is of the order–disorder type, it is necessary to analyze the shape of the potential well and verify that the well depth satisfies the condition $U_w \gg kT_c$.

The strong temperature dependence of the parameters a and R_{min}^2 observed in this study is an unexpected result.[2] It follows from Figs. 4 and 5 that, for the samples with $x \geq 0.7$, the parameter a decreases and R_{min}^2 increases as the temperature increases, with the potential-well depth $U_w = aR_{min}^4$ remaining practically unchanged in this case. It should be noted that these sufficiently strong changes in the potential parameters do not lead to a noticeable change in the mean-square atomic displacement from a lattice site. The calculation of the temperature dependence of the quantity

$$\langle r^2 \rangle = \int \rho(\mathbf{r})\mathbf{r}^2 d\mathbf{r} \qquad (6)$$

shows that the displacement of the "center of gravity" of the distribution function does not exceed 0.04 Å (12%) as the temperature T increases from 80 to 300 K. One of the reasons for this variation is the thermal expansion of the crystal, although this reason is not likely to be the only one.

As follows from Fig. 4, the extrapolation of the $a(T)$ dependences for the samples with $x \geq 0.7$ to high temperatures predicts negative values for the parameter a at the Curie temperature ($T_x \approx 700$ K for the sample with $x = 1$ and ≈ 500 K for the sample with $x = 0.7$). It was shown in [3] that, for displacement-type PTs ($s \ll 1$), there is a direct relation between the coefficient of the fourth power of the order parameter (A_{th}) in the thermodynamic potential and the coefficient a in the microscopic potential. Therefore, the negative values of a could indicate that the PT is of the first order (which is the case if $A_{th} < 0$). However, in our case ($s \sim 1$), the relation between the coefficients A_{th} and a is much more complicated [20]. Unfortunately, we cannot determine the sign of A_{th} on the basis of the obtained parameters of the microscopic potential, because, in order to estimate A_{th}, we need to know the values of the sixth-order coefficients in the expansion of $V_{loc}(\mathbf{r})$, but they were neglected in our analysis of the data. In addition, the inclusion of the molecular field (also neglected in this study) can affect the obtained results. These problems require further studies.

---

[2] Because of the three-dimensional character of the problem under study, estimating the statistical errors in the experimental determination of the parameters is an independent complicated problem. At present, we can estimate the errors from the scatter of the parameters for spectra recorded under the same conditions.
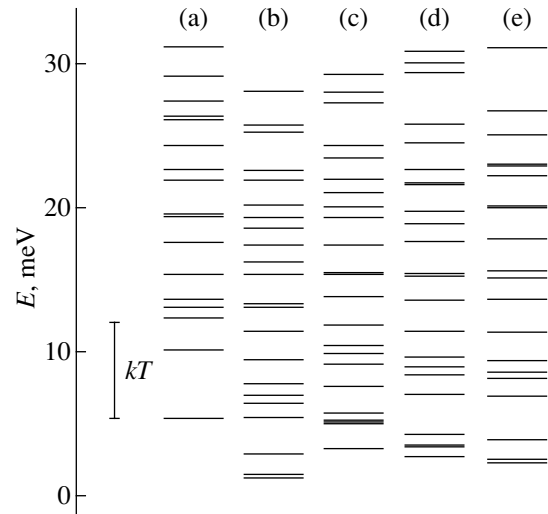
Fig. 7. Vibration spectrum of a Ge atom in potential wells obtained in the classical approximation and using the quantum-mechanical approach for a $Sn_{0.3}Ge_{0.7}Te$ sample at 80 K.

5. VERIFICATION OF THE APPLICABILITY OF THE CLASSICAL APPROXIMATION

The data processing described above was based on the use of the classical approximation. By solving the problem by a rigorous method (using quantum mechanics) and verifying that both solutions coincide, one can justify the application the classical approximation.

To calculate the distribution function by the rigorous method, it is necessary to solve the Schrödinger equation for the strongly anisotropic and anharmonic potential $V(\mathbf{r})$ obtained in the classical approximation and find its wave functions $\{\psi_i\}$ and eigenvalues $\{E_i\}$. The Schrödinger equation was solved by a numerical variational method in one octant on a lattice with dimensions $121 \times 121 \times 121$. The symmetry of the solution was taken into account using boundary conditions. The energy spectrum of the Ge atom in the potential well obtained in the classical approximation is shown in Fig. 7a. It is seen that the lowest energy level is 5.3 meV above zero (the value of the potential $V(0)$ is taken as the zero of energy), i.e., approximately 30 meV above the potential minimum. This means that the atom is not localized in a minimum, although the potential has many minima. We assume that the strong "expulsion" of energy levels is a consequence of the strong anisotropy in our problem: the localization of the atomic motion in "channels" extended in the $\langle 111 \rangle$ directions (Fig. 3) leads to a considerable increase in the atom kinetic energy. Thus, the quantum effects in our problem turn out to be unexpectedly important.

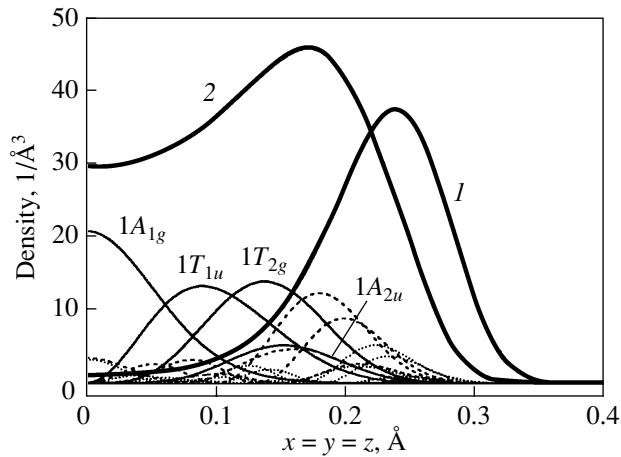In Fig. 8, the distribution function obtained from processing the EXAFS spectrum for a $Sn_{0.3}Ge_{0.7}Te$

Fig. 8. Comparison of (*1*) the distribution function in a $\langle 111 \rangle$ direction obtained by processing the EXAFS spectrum for $Sn_{0.3}Ge_{0.7}Te$ samples at 80 K in the classical approximation and (*2*) the quantum-mechanical distribution function obtained using twenty wave functions for the potential found in the classical approximation. The thin solid, dashed, and dotted lines correspond to the contributions of the first twelve wave functions to the quantum-mechanical distribution function.

sample at 80 K in the classical approximation ($\rho(\mathbf{r}) \sim \exp[-V(\mathbf{r})/kT]$) is compared with the function

$$\rho(\mathbf{r}) = \frac{1}{Z}\sum_i e^{-E_i/kT}|\psi_i(\mathbf{r})|^2, \quad Z = \sum_i e^{-E_i/kT}, \quad (7)$$

calculated by quantum statistics methods using the first twenty wave functions corresponding to the same potential $V(\mathbf{r})$. As follows from Fig. 8, the graphs of these distribution functions differ essentially in both the shape and the position of the maximum. This demonstrates that, in studying multiwell potentials, the classical approximation is inapplicable to the processing of EXAFS spectra, at least those obtained at low temperatures.

6. QUANTUM-MECHANICAL APPROACH

Under a rigorous quantum-mechanical approach with quantum effects consistently taken into account, the problem of the EXAFS data processing becomes much more complicated. For parametrized potential (5), it is necessary first to calculate the wave functions and eigenvalues and substitute them into Eq. (7). Then, the obtained distribution function $\rho(\mathbf{r})$ can be inserted in Eq. (3) to calculate the EXAFS function $\chi(k)$. By varying the parameters of the potential and repeating quantum-mechanical calculations each time, one can find (using one of the minimization algorithms) the set of parameters for which the rms discrepancy between the theoretical and experimental EXAFS spectra becomes minimum.

Because the proposed approach is very time-consuming, we should perform calculations using a minimum set of wave functions to estimate the potential parameter values. If the EXAFS spectra are measured at a sufficiently low temperature, then only several lowest energy levels are occupied in the vibration spectrum. However, because the vibration spectrum depends on the potential parameters in a complicated way and because the number of wave functions to be taken into account is unknown, we solved the problem using the iteration method. We processed the same EXAFS spectra of the $Sn_{0.3}Ge_{0.7}Te$ and GeTe samples (recorded at the lowest temperature, 80 K) until the energy of the previously neglected levels became approximately $2kT$ greater than the energy of the ground state.

First, we assumed that, in order to describe the motion of the Ge atom, it suffices to take into account only the lowest $1A_{1g}$ level (corresponding to the zero-point energy).[3] The vibration spectrum for the potential determined in this approximation is shown in Fig. 7b, and the values of the potential parameters, in the table. Because the splitting of the low-lying excited energy levels is only $\Delta E = 0.346$ meV $\ll kT$ and, consequently, these states are approximately equally excited, it is clear that our approximation is not good.

Next, we considered the problem in which the four lowest levels ($1A_{1g}$, $1T_{1u}$, $1T_{2g}$, $1A_{2u}$) are included and the threefold degeneracy of the T_{1u} and T_{2g} levels is taken into account. The results of these calculations are given in Fig. 7c and in the table. Because the $2A_{1g}$ level (the lowest level not taken into account in this approximation) turned out to be higher than the ground level by only 2.466 meV (which is less than kT), it is clear that one should include a larger number of wave functions.

Calculations with the inclusion of eight wave functions ($1A_{1g}$, $1T_{1u}$, $1T_{2g}$, $1A_{2u}$, $2A_{1g}$, $2T_{1u}$, $2T_{2g}$, $2A_{2u}$) are quite acceptable, because the nearest level not taken into account ($3A_{1g}$) is higher that the ground level by 6.989 meV, which is slightly greater than kT (see Fig. 7d and table).

Finally, calculations with the inclusion of twelve wave functions (the $3A_{1g}$, $3T_{1u}$, $3T_{2g}$, and $3A_{2u}$ states are added) yield the most reliable results; the nearest level not taken into account is 13.356 meV higher than the ground state (see Fig. 7e and table).

Now, we consider the character of the variations in the potential parameters caused by the inclusion of a greater number of wave functions and compare these parameters with those obtained in the classical approximation. As is seen from the table, the agreement between the theoretical and experimental curves (char-

---

[3] In the notation for wave functions, the first numeral is the principal quantum number (it determines the number of zeros in the radial part of the wave function, just as in the hydrogen atom) and the symbols following it indicate the angular symmetry of the function.

Parameters of the potential and the potential-well depth obtained from processing the EXAFS spectra of $Sn_{0.3}Ge_{0.7}Te$ and GeTe at 80 K within the classical approximation (CA) and the quantum-mechanical approach using various numbers of wave functions

Number of wave functions	a, eV/Å^4	R^2_{min}, Å^2	d, eV/Å^4	U_w, meV	Σ
		$Sn_{0.3}Ge_{0.7}Te$			
CA	0.8476	0.1717	–137.19	24.91	0.016752
1	0.6924	0.2321	–85.60	37.30	0.017427
4	0.5032	0.2553	–80.21	32.80	0.017309
8	0.7863	0.2266	–115.28	40.36	0.017153
12	0.9662	0.2166	–142.77	45.32	0.017078
		GeTe			
CA	1.4864	0.1414	–172.91	29.73	0.014853
1	1.0996	0.1858	–95.21	37.95	0.015388
4	0.9212	0.1993	–109.07	36.61	0.015220
8	1.4183	0.1763	–133.83	44.08	0.015058
12	1.7146	0.1686	–154.39	48.74	0.015041

acterized by the rms deviation Σ) improves as the number of wave functions increases. The quantum character of atomic motion most strongly affects the position of the potential minimum R_{min} and the potential-well depth U_w (see table). The well depth calculated with the inclusion of twelve wave functions is 60–80% greater than that obtained in the classical approximation. The values of d in both approaches turn out to be close, and the value of a is slightly greater in the quantum-mechanical approach.

The quantum-mechanical calculation shows that, in all cases considered, the energy of the $1A_{1g}$ ground state is positive; i.e., the Ge atom is not localized in a minimum. Nevertheless, the maxima of the atomic distribution function are displaced from the lattice site (Fig. 9). The transition rate from one off-center position to another can be estimated from the splitting of the $1A_{1g}$–$1A_{2u}$ levels, which is $\Delta E = 0.387$ meV for $Sn_{0.3}Ge_{0.7}Te$ and 0.142 meV for GeTe and corresponds to a "lifetime" of a particle in one minimum $\tau = \hbar/\Delta E \approx (1.7–4.6) \times 10^{-12}$ s. In this case, the typical transition frequency is one order of magnitude less than the characteristic frequency of the soft mode.

7. DISCUSSION

As shown above, the shape of the potential well found using the classical and quantum-mechanical approximations is qualitatively the same and the well parameters do not differ significantly. Although the quantum-mechanical problem was solved only for one temperature value, it can be expected that the pattern of the temperature dependences of the parameters a and R^2_{min} remains qualitatively the same in both the classical and quantum-mechanical approaches. This conclu-

sion is based on the fact that, first, the potential parameters in both approaches must coincide in the high-temperature limit and, second, the difference between the parameters at 80 K in both approaches is less than the change in these parameters over the temperature range 80–300 K in the classical approach.

One would think that the use of the quantum-mechanical approach in the data processing only refines the values of the potential parameters. However, this is not the case; namely, this approach leads to a qualitatively new result concerning the character of the particle motion. According to the classical approach to the problem of motion of off-center atoms, their reori-
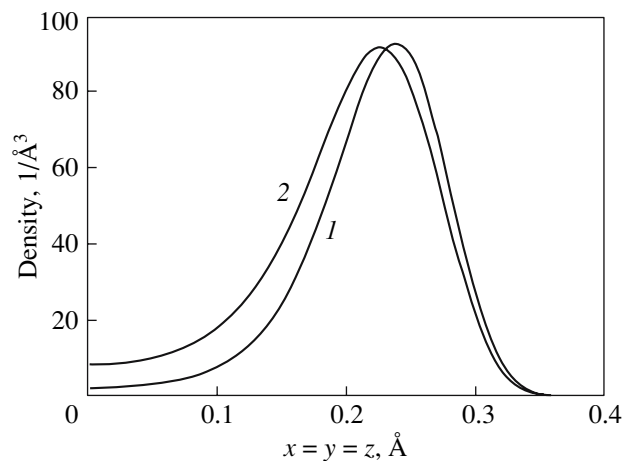

Fig. 9. Comparison of the distribution functions along a $\langle 111 \rangle$ direction found by processing the EXAFS spectrum for a $Sn_{0.3}Ge_{0.7}Te$ sample at 80 K (*1*) in the classical approximation and (*2*) using the quantum-mechanical approach. The potential parameters are taken from the last two rows of the table.

entation occurs by overcoming the potential barriers separating different wells. An example of this type of motion is the motion of an off-center Li atom in $KTaO_3$. Measurements of the relaxation time of the Li atom by the NMR and dielectric relaxation methods have shown that the dipole reorientation is thermally activated with an activation energy of 0.085 eV [21]. The results obtained in this work for the off-center Ge atom in $Sn_{1-x}Ge_xTe$ show that the lower vibration levels of this atom are located near the potential maximum at $\mathbf{r} = 0$ within several millielectronvolts. Consequently, the atomic transitions from one off-center position to another occur either by tunneling or by passing over barriers. For this reason, it can be expected that, in the limit $T \longrightarrow 0$, the dipole reorientation rate will remain high and, hence, the dynamics of the off-center atom will not "frozen".

The distinctions between the dynamics of off-center Li atoms in $KTaO_3$ and off-center Ge atoms in $Sn_{1-x}Ge_xTe$ indicate that these atoms are examples of static and dynamic impurities, respectively (similar to Jahn–Teller impurities). For a Li atom, the quantum effects are insignificant due probably to the fact that the off-center displacement of this atom is 1.26 Å (which is three times greater than that of the Ge atom in $Sn_{1-x}Ge_xTe$) and, therefore, the probability of tunneling transitions between the wells is low for this atom (the "lifetime" of the atom in a minimum is ~10^4 s [22]). In this connection, it would be interesting to study the intermediate case of an off-center Ge atom in PbTe, whose displacement is 0.7 Å [10].

The dynamic character of the off-center Ge atom in $Sn_{1-x}Ge_xTe$ explains the illusory contradiction between the EXAFS data demonstrating the existence of off-center atoms and the physical properties showing that the PTs in $Sn_{1-x}Ge_xTe$ are of the displacement type.

Our quantum-mechanical calculations have been performed without inclusion of the molecular field and, therefore, describe the motion of the system above the PT point. The case of a nonzero molecular field will be studied in a later paper. Nevertheless, the conclusion that it is necessary to take into account the quantum character of the atomic motion in analyzing the properties of a system with off-center atoms is an important result of this study.

8. CONCLUSIONS

We have proposed an approach that makes it possible to determine the shape of the three-dimensional potential of an off-center atom and the parameters of the microscopic ferroelectricity model from EXAFS data. For $Sn_{1-x}Ge_xTe$ solid solutions with $x \geq 0.4$, we have found the temperature and composition dependences of the multiwell-potential parameters for a Ge atom in the classical approximation. The potential-well depth varies from 20 to 40 meV depending on the Ge

content in the sample. It has been shown that the phase transition (PT) in these crystals is intermediate between the displacement and order–disorder types.

Analyzing the applicability of the classical approximation has revealed that it is necessary to take into account quantum effects in determining the parameters of potential wells in strongly anisotropic systems, such as off-center Ge atoms in $Sn_{1-x}Ge_xTe$. An algorithm has been proposed for data processing in which the theoretical EXAFS spectrum and the distribution function are calculated from strict formulas of quantum statistics using calculated wave functions. The fact that the lower vibration energy level of the Ge atom coincides with the maximum energy in the potential well to within several millielectronvolts is an unexpected result of our quantum-mechanical calculations. The high probability of an off-center atom tunneling through or passing over the barrier between the potential-well minima prevents dipole reorientations from being frozen at low temperatures. This special feature explains the illusory contradiction between the physical properties showing the closeness of the PTs in $Sn_{1-x}Ge_xTe$ to the displacement type and the EXAFS data demonstrating the large displacements of Ge atoms from the lattice sites above the Curie temperature.

REFERENCES

1. B. E. Vugmeister and M. D. Glinchuk, Rev. Mod. Phys. **62**, 993 (1990).

2. A. Brause and R. Cowley, *Structural Phase Transitions* (Taylor and Francis, London, 1981; Mir, Moscow, 1984).

3. B. A. Strukov and A. P. Levanyuk, *Ferroelectric Phenomena in Crystals* (Nauka, Moscow, 1995; Springer, Berlin, 1998).

4. J. N. Bierly, L. Muldawer, and O. Beckman, Acta Metall. **11**, 447 (1963).

5. R. Clarke, Phys. Rev. B: Condens. Matter **18**, 4920 (1978).

6. I. Hatta and W. Rehwald, J. Phys. C: Solid State Phys. **10**, 2075 (1977).

7. W. Rehwald and G. K. Lang, J. Phys. C: Solid State Phys. **8**, 3287 (1975).

8. E. F. Steigmeier and G. Harbeke, Solid State Commun. **8**, 1275 (1970).

9. B. A. Bunker, Q. T. Islam, and W.-F. Pong, Physica B (Amsterdam) **158**, 578 (1989).

10. Q. T. Islam and B. A. Bunker, Phys. Rev. Lett. **59**, 2701 (1987).

11. O. Hanske-Petitpierre, Y. Yacoby, J. Mustre de Leon, E. A. Stern, and J. J. Rehr, Phys. Rev. B: Condens. Matter **44**, 6700 (1991).

12. N. Sicron, B. Ravel, Y. Yacoby, E. A. Stern, F. Dogan, and J. J. Rehr, Phys. Rev. B: Condens. Matter **50**, 13168 (1994).

13. N. Sicron, Y. Yacoby, E. A. Stern, and F. Dogan, J. Phys. IV **7**, 1047 (1997).

14. B. Ravel, E. Cockayne, M. Newville, and K. M. Rabe, Phys. Rev. B: Condens. Matter **60**, 14632 (1999).

15. V. Shuvaeva, Y. Azuma, K. Yagi, H. Terauchi, R. Vedrinski, V. Komarov, and H. Kasatani, Phys. Rev. B: Condens. Matter **62**, 2969 (2000).

16. G. Bunker, Nucl. Instrum. Methods Phys. Res. **207**, 437 (1983).

17. P. A. Lee, P. H. Citrin, P. Eisenberger, and B. M. Kincaid, Rev. Mod. Phys. **53**, 769 (1981).

18. A. I. Lebedev, I. A. Slichinskaya, V. N. Demin, and I. H. Munro, Phys. Rev. B: Condens. Matter **55**, 14770 (1997).

19. J. Mustre de Leon, J. J. Rehr, S. I. Zabinsky, and R. C. Albers, Phys. Rev. B: Condens. Matter **44**, 4146 (1991).

20. M. E. Lines, Phys. Rev. **177**, 797 (1969).

21. F. Borsa, U. T. Höchli, J. J. van der Klink, and D. Rytz, Phys. Rev. Lett. **45**, 1884 (1980).

22. W. Kleemann, V. Schönknecht, D. Sommer, and D. Rytz, Phys. Rev. Lett. **66**, 762 (1991).

Translated by L. Kul'man